Shock induced flow-separation in hypersonic intakes at off-design conditions

Rachit Singh[1] and Krishnendu Sinha.[2]
Indian Institute of Technology Bombay, Mumbai-400076, Maharashtra, India

High-speed turbulent flow in hypersonic intakes encounters flow-separation due to shock-boundary layer interaction. Presence of separation bubble changes the pressure distribution over the surface which can lead to deterioration of aerodynamic performance of intake and thus jeopardize the stability of vehicle. In this study, we employ the physics-based shock-unsteadiness $k-\varepsilon$ model to compute separation bubble size in a mixed compression two-ramp intake. The design point Mach number of 6 at 30 km altitude with zero angle of attack is considered. Changes in separation bubble length is analyzed at different off-design conditions by varying the flight Mach number, angle of attack and cruise altitude. The changes observed in the separation length by variation of above flight parameters is studied in terms of the physically relevant canonical parameters of upstream Mach number, Reynolds number Re_δ and the ratio of wall to recovery temperature. CFD simulations are performed for the entire range of canonical and flight parameters. Wall-to-recovery-temperature ratio is found to be an important governing parameter for separation length studies. The largest shock-induced separation is observed for the case of off-design flight Mach number of 8. The corresponding effect on the lift and drag generated by the hypersonic intake are quantified.

Nomenclature

Re = Reynolds number based on characteristic length

Re_δ = Reynolds number based on boundary layer thickness

Re_θ = Reynolds number based on momentum thickness

M = Mach number

---

[1] Postgraduate student, Department of Aerospace Engineering.
[2] Professor, Department of Aerospace Engineering, and AIAA Member.

T = Temperature (K)

ρ = Density (kg/m^3)

p = Pressure (Pa)

C_f = Coefficient of skin-friction

S = Separation point

R = Reattachment point

k = Turbulent kinetic energy (m^2/s^2)

ε = Dissipation of turbulent kinetic energy (m^2/s^3)

ω = Rate of dissipation of turbulent kinetic energy (1/s)

z = Altitude (km)

α = Angle of attack

F = Force (N)

θ = Ramp/Deflection angle (degree)

β = Shock angle (degree)

R_1 = First ramp length (m)

R_2 = Second ramp length (m)

dx = grid thickness (m)

x = distance in stream-wise direction (m)

y = distance in wall-normal direction (m)

δ^* = displacement boundary layer thickness (m)

δ = boundary layer thickness (m)

L^* = Normalized interaction length

S_e^* = Normalized shock-strength

L_{sep} = Separation length

L_{int} = Interaction length

Subscripts

1 = Free-stream or station-1

2	=	Station-2
3	=	Station-3
w	=	Wall
r	=	Recovery for recovery temperature
sep	=	Separation
reat	=	Reattachment

I. Introduction

Interaction of shock wave with boundary layer plays an important role in the design of hypersonic vehicles as it induces mechanical and thermal load on vehicle surface which are critical factors influencing the aerodynamic design and performance of vehicle. The control surfaces are frequently dominated by shock boundary layer interactions [1] which can cause the flow to separate leading to formation of separation bubble. Flow-separation modifies the wall-pressure distribution over the vehicle surface which deteriorates the aerodynamic performance of control surface leading to loss of control surface effectiveness and vehicle instability [1, 2] . In internal flows, presence of separation bubble may lead to catastrophic changes leading to intake buzz or even unstart in worst case [3, 4] .

Figure-1 shows the schematic of a scramjet engine which consists mainly of intake, combustor, and nozzle. At the intake, shock is formed at the corner between the two ramps due to abrupt disruption of flow and it interacts with the boundary layer. Depending on the strength of interaction, a separation bubble is formed for strong interactions as shown in figure-2 and for weak interactions swelling of the boundary layer is observed without any flow-separation. In weak interactions, the pressure distribution is close to inviscid solution whereas for strong interactions, the pressure distribution deviates strongly from the inviscid solution [3]. Pressure is seen to rise upstream of separation point (S), reaches plateau inside the separation bubble and again increases at the reattachment point. The length of separation bubble is the distance between the separation (S) and re-attachment (R) point.

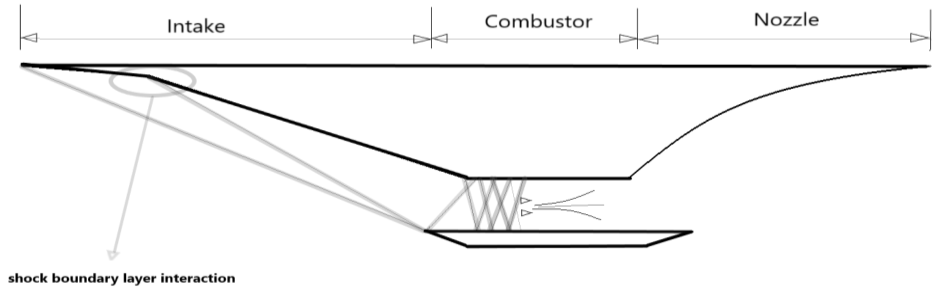

Figure 1 : Schematic of scramjet engine showing shock-boundary layer interactions at corner in Intake.

Extensive research has been carried out in the past, both experimental and computational, in order to understand the physics of flow separation associated with shock-wave interacting with boundary layer for both laminar and turbulent flows across compression corner. Pasha et al. [5] did a parametric study of changes in separation length with respect to various parameters and observed that the size of separation length increases with increase in Reynolds number Re_δ (Reynolds number based on boundary layer thickness) and wall-temperature while Mach number shows an opposite effect. Bernardini et al. [6] investigated the effect of wall-temperature on the behavior of oblique shock-wave/turbulent boundary layer interactions for supersonic flow over a compression ramp geometry using DNS and concluded that wall cooling leads to considerable reduction in the size of the separation bubble while the opposite holds true for wall heating cases. John et al. [7] studied the laminar boundary layer separation in the presence of ramp induced shock-waves for different Mach numbers and wall-temperatures using RANS computations. They observed that the size of separation bubble decreases as the Mach number increases and as the wall-temperature increases, the viscosity increases leading to increase in thermodynamic boundary layer thickness and in separation length. Morgan et al. [8] carried out a parametric investigation of oblique shock impinging on a supersonic turbulent boundary layer to study the effect of ramp angle and Reynolds number. It was found that stronger shock, due to increased ramp angle, leads to wider interaction region and with respect to Reynolds number, the separation length was found to be not much affected. Marini et al. [9] studied the effect of ramp angle and wall-temperature on separation length using RANS computations for laminar flow over a compression ramp. The separation length was found to increase with increase in wall-temperature and ramp angle. Katzer et al. [10] carried out a numerical analysis of an oblique shock interacting with an adiabatic flat-late in a laminar flow for a range of Mach numbers and Reynolds numbers. It was found that increasing the Reynolds number increases the length of separation bubble and with respect to Mach number, the opposite effect was observed. Roshko and Thomke [11] did an experimental investigation on separation of turbulent boundary layer over flare geometry to study the effect of Mach number, Reynolds number and flare angle. They found that the separation length, normalized by the boundary layer thickness, decreases with increase in Reynolds number Re_δ and Mach number. The normalized separation length was found to increase with increase in flare angle. Elfstorm et al. [12] carried an experimental investigation on shock turbulent boundary-layer interaction at wedge-compression corner using pressure measurements along the wall for different wall-temperatures, Reynolds numbers and Mach numbers. The separation length was found to increase with increase in ramp angle and wall-temperature. Increase in Mach number led to decrease in separation length. With respect to Reynolds number, the extent of separation region was found to increase with Re_δ and the incipient separation angle reduces slightly. Needham and Stollery [13] carried out experiments for a range of Mach numbers and Reynolds number to study its effect on flow separation for wedge-compression corner and shock-impinging over flat-plate geometry and found that the extent of separation increases with increase in Reynolds number and decrease in Mach number in laminar flow regimes.

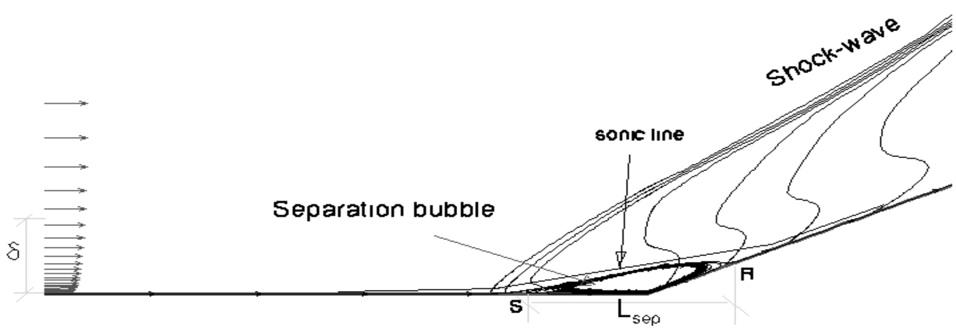

Figure 2 : Schematic showing the separation bubble, incoming boundary layer thickness δ and the shock-wave in the computational domain.

The past studies on flow-separation in supersonic flows mainly dealt with the study of separation length with respect to various flow parameters at ground experimental test facilities. The computational results were validated using these experimental data and further extended to conditions that cannot be replicated in experimental test facilities. However, as pointed by Miller et al. [14] , the behavior of separation length with respect to different flight conditions is least explored and hence there is a limited understanding in this area. With this objective, to study the behavior of separation length at different flight conditions, a parametric study is carried out for following three flight parameters - flight Mach number, angle of attack and cruise altitude. Justifying the trend observed in separation length changes for varying flight conditions is not an easy task as variation in one flight parameter leads to changes in multiple parameters across the shock-wave and thus the observed changes in separation length are due to the cumulative effect of multiple parameters acting simultaneously. This makes it difficult to identify the effect of individual parameter on separation length. Hence it is important to study how the separation length gets affected by each of the individual parameters as this would assist in justifying the trend observed while varying the flight parameters. Morgan et al. [8] commented that - *Although there have been a number of previous computational studies that look at OSTBLI (Oblique shock turbulent boundary layer interactions), very few of these focus on simulating more than a single set of flow conditions, and those that do generally vary more than one flow parameter at a time, which makes it difficult to associate trends with particular flow parameters*.

The second objective of this work is to study the effect of canonical (individual) parameters. The flight parameters considered in this work, are found to be the function of - Mach number, pressure, temperature and density. Apart from these, wall-temperature is also an important parameter and hence considered as part of the canonical parameter. Following parameters are considered in the canonical study - (i) Mach number, (ii) wall-to-recovery-temperature ratio (T_w/T_r) as it takes into account both wall-temperature (T_w) as well as free-stream temperature (T_∞) since recovery temperature $T_r = T_\infty\left(1+\frac{1+\gamma}{2}rM_\infty^2\right)$ and (iii) Reynolds number Re_δ as the separation length is normalized with respect to boundary layer property - displacement boundary layer thickness δ^*. For this, a canonical case of compression corner, shown in figure-3 as part of the scramjet, is considered as a model problem as this allows us to do a controlled study where only canonical parameter can be varied such that all other parameters remain constant. The conditions at station-2 are used as inlet conditions for the simulations. The conclusion drawn from the study of these canonical cases (wall-temperature, Mach number and Reynolds number) would be helpful to understand/justify the observed trend in separation length variation with respect of various flight parameters.

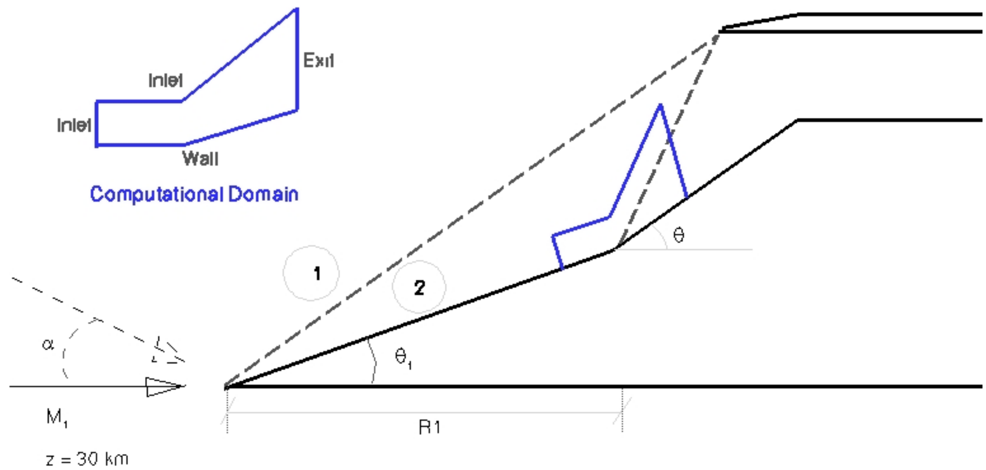

Figure 3 : Schematic of scramjet with the computational domain.

In scramjet intakes, the presence of shock-induced separation in itself is not as critical as the modifications it does to the pressure distribution over the ramp surface. The modified pressure over the surface is more critical than the presence of separation bubble itself, as it spoils the aerodynamic efficiency leading to loss of control surface effectiveness and vehicle instability [1, 2] . The last objective is to quantify this effect of shock-induced separation on the wall-pressure distribution. For this, the pressure lift and drag acting over the two ramps is computed using inviscid relations and is compared with the CFD computed pressure lift and drag to find the percentage difference between the two. This percentage difference over the first two ramps shows the effect of separation bubble as well as separation shock and would lead to the identification of the worst case scenario of all the off-design condition operation.

II. Methodology

The standard turbulence models ($k-\varepsilon$ and $k-\omega$) predicts delayed flow-separation [15,16] and the application of shock-unsteadiness correction [17] moves the separation point closer to the experiments thereby providing better predictions for flow over both compression corner [1] and shock-impingement [2] geometry. However, for lower deflection angles, the effect of the correction term diminishes and thus it does not alter the separation predictions for weakly interacting flows where the standard models give reasonably good predictions. In this work, Favre-averaged Navier-stokes equations [18] are solved for mean flow and shock-unsteadiness modified $k-\varepsilon$ turbulence model

[17] is used for turbulence closure. The computations are done using an in-house code which is well validated and used in various applications [15, 19, 20] . The governing equations are discretized in finite volume formulation wherein the convective fluxes are solved using low-dissipation modified Steger-Warming flux vector splitting method [21] . The viscous fluxes and the turbulent source terms are solved using second order central difference method. The implicit DPLR (Data Parallel Line Relaxation) method [22] is used to integrate in time to achieve steady-state solution. Inlet profiles for the computations are obtained from separate simulations of first ramp wherein the free-stream conditions are applied at the inlet and the initial condition for turbulent variables k and ε are computed using relations given in reference [23] . No-slip and zero normal pressure gradient is applied to the wall and extrapolation boundary conditions are applied to the exit plane. A structured grid with exponential stretching in the y-direction at wall and in the x-direction at the corner between the two ramps is used. The Mach number, density, and temperature at the design point conditions are M_1 = 6, ρ_1 = 0.01802 kg/m^3 and T_1 = 256.56 K which correspond to an altitude of 30 km.

At the junction between the two ramps (see schematic in figure-3), an oblique shock is formed and the flow gets separated inside the boundary layer leading to formation of separation bubble. Figure-2 shows schematic of separation bubble where L_{sep} is length of separation bubble (distance between separation S and re-attachment R) and δ^* is the incoming displacement boundary layer thickness. The total inviscid force acting on two ramps is given as,

$$F_{inviscid} = p_1R_1 + p_2R_2 \qquad (1)$$

where R_1 and R_2 are length of first and second ramp while p_1 and p_2 are pressure acting at first and second ramp respectively. The total CFD computed force acting on the two ramps is given by,

$$F_{CFD} = \sum_1^n dx_i p_i \qquad (2)$$

where P_i is pressure acting at given cell i and dx_i is the distance over which the pressure p_i acts. In order to compute the lift and drag force due to the above pressure, the components in horizontal direction (Drag force F_x) and in vertical direction (Lift force F_y) is computed as given below,

$$F_y = \sum_1^n dx_i P_i cos\theta_i \qquad (3)$$

$$F_x = \sum_1^n dx_i P_i sin\theta_i \qquad (4)$$

where θ_i is ramp angle at a given location which is constant for a given ramp. The inviscid lift and drag forces are calculated using the same equations as above by taking the horizontal and vertical components of the inviscid force given in equation-1.

In order to do the validation of results, an experiment on supersonic turbulent flow over compression corner of varying ramp angles by Settles et al. [24] is considered. The free-stream conditions given in the experiments were M_∞ = 2.83, P_∞ = 23.9 kPa, T_∞ = 103 K and ρ_∞ = 0.8096kg/m^3. The ramp angles ranged from θ = 16, 20, 24 º and the incoming boundary layer thickness was δ_0= 2.3 cm for all the cases. The free-stream Reynolds number was Re = 7.3 x 10^7 /m. The computed pressure distribution results are compared with the above experimental data. Figure-4a shows the validation giving comparison of computed results with experimental data of Settles et al. [24] for 24º ramp angle case where strong interaction is seen and observed separation length is largest compared to all cases. The stream-wise direction is normalized by incoming boundary layer thickness δ. The normalized pressure distribution is compared with experimental data as well as inviscid solution obtained using Rankine-Hugonoit relations. The first pressure rise (upstream influence) occurs near the separation point and second pressure rise occurs just downstream of corner. The plateau region (between the two pressure rises) indicates the region of flow-separation.

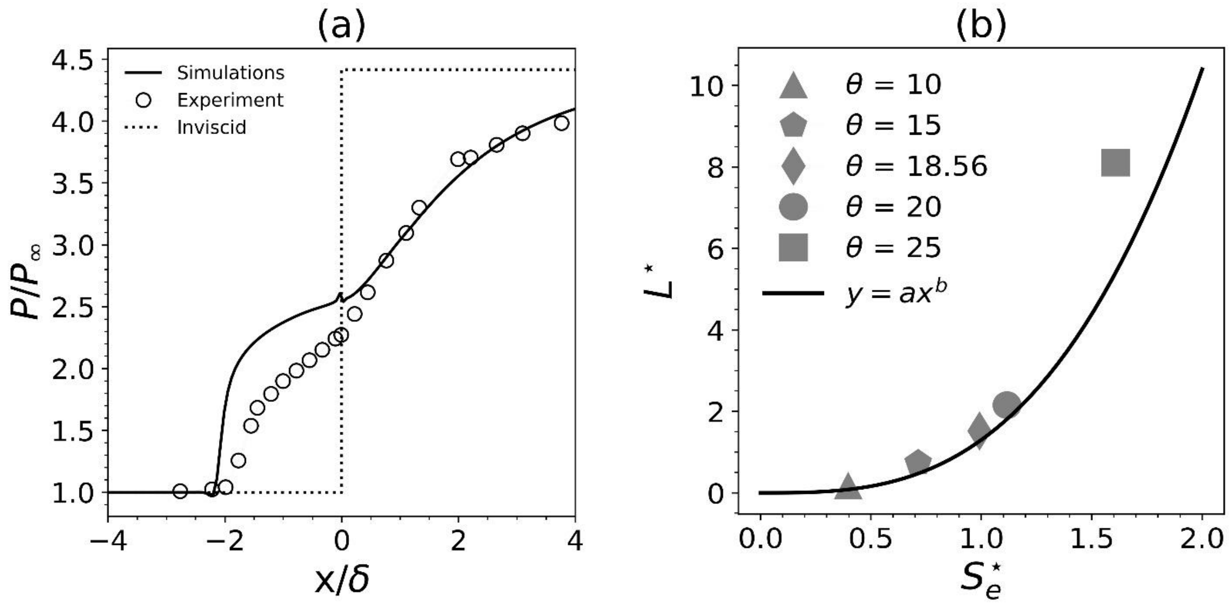

Figure 4 : Comparison of (a) computed wall-pressure for 24º case with the experimental data of Settles et al. [24] and (b) computed separation length for different angles with scaling law of Souverein et al. [25].

According the scaling law proposed by Souverein et al. [25], the normalized interaction length (L*) when plotted against the normalized shock-strength (S_e^*), all the data is observed to follow the curve given by $y = ax^b$ where a = 1.3 and b = 3 are constants in the equation.

$$L^* = \frac{L_{int}}{\delta_0^*}\frac{sin\beta\ sin\theta}{\sin(\beta-\theta)} \qquad (5)$$

$$S_e^* = \frac{2k}{\gamma}\frac{P_2/P_1 - 1}{M_e^2} \qquad (6)$$

The interaction length (L_{int}) is the observed upstream shift of shock-wave from the inviscid case due to swelling of the boundary layer. δ_0^* is displacement thickness upstream of the interaction, β is shock-angle and θ is deflection or ramp angle. The ratio $P_2/P_1$is the pressure jump across the shock, M_e^2 is free-stream or edge Mach number and k is a constant with value of k = 3 for Re_δ < 1e+5 and k = 4 for Re_δ ≥ 1e+5 where is Reynolds number based on momentum thickness. The present results obtained for different ramp angles (10, 15, 20, 25 º) at M = 4.097, T = 425.55 K and ρ= 0.05385 kg/m^3 are presented in Figure-4b and designated by filled circles with a nearby value representing the ramp angle. All data follow the best fit curve proposed by Souverein et al [25].

Figure-5 shows the comparison of present results with results of Sinha et al. [15] for 16, 20 and 24 º ramp angle case. The stream-wise direction is normalized by incoming boundary layer thickness δ. The upstream influence (first pressure rise due to separation shock) is observed at x/δ ~ -2 location for 24 degree case and it move further downstream with decrease in ramp angle as seen in Figure-5a. The upstream influence is followed by plateau (constant pressure in the re-circulation region) and then a second pressure rise, due to reattachment shock, is observed at downstream of corner. The pressure jump increases with increase in ramp angle due to increase in shock-strength. Figure-5b shows the comparison of computed skin-friction distribution for same ramp angle cases. The location (at x/δ ~ -2 for 24 degree case) where value of skin-friction starts to fall indicates the upstream influence. The flow gets separated at x/δ ~ -1.5 location for 24 degree case, where the skin-friction takes zero value and this location is denoted as separation point (S). The flow gets re-attached, at x/δ ~ +1.25 for 24 degree case, where the skin-friction reaches back to zero from negative values and this location is denoted as re-attachment point (R). The region between the separation and re-attachment point indicates the re-circulation region. The separation length is taken as the distance between the separation (S) and re-attachment (R) points and is normalized with incoming displacement boundary layer thickness δ*. It is seen that as the ramp angle decreases the separation length (distance between separation and re-attachment point) decreases due to decrease in shock-strength with decrease in ramp angle.

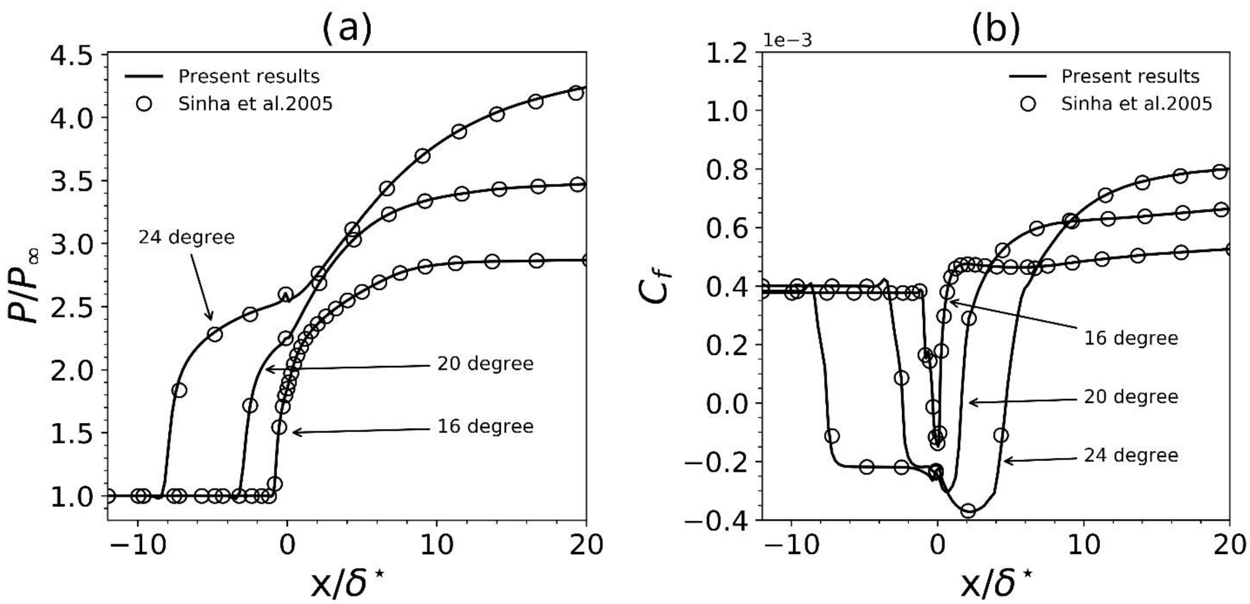

Figure 5 : Comparison of computed wall-pressure and skin-friction distribution with the computational results of Sinha et al. [15].

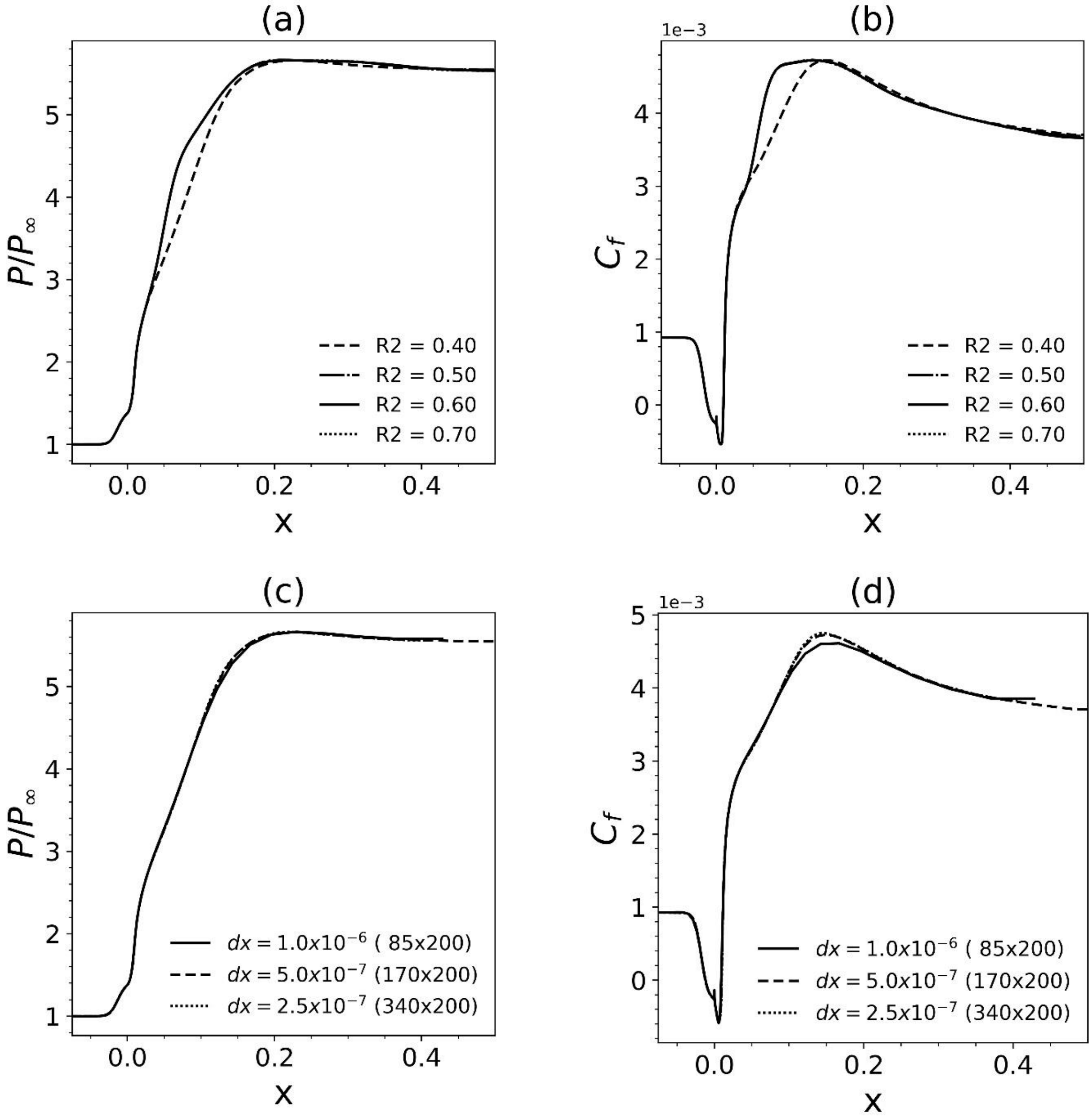

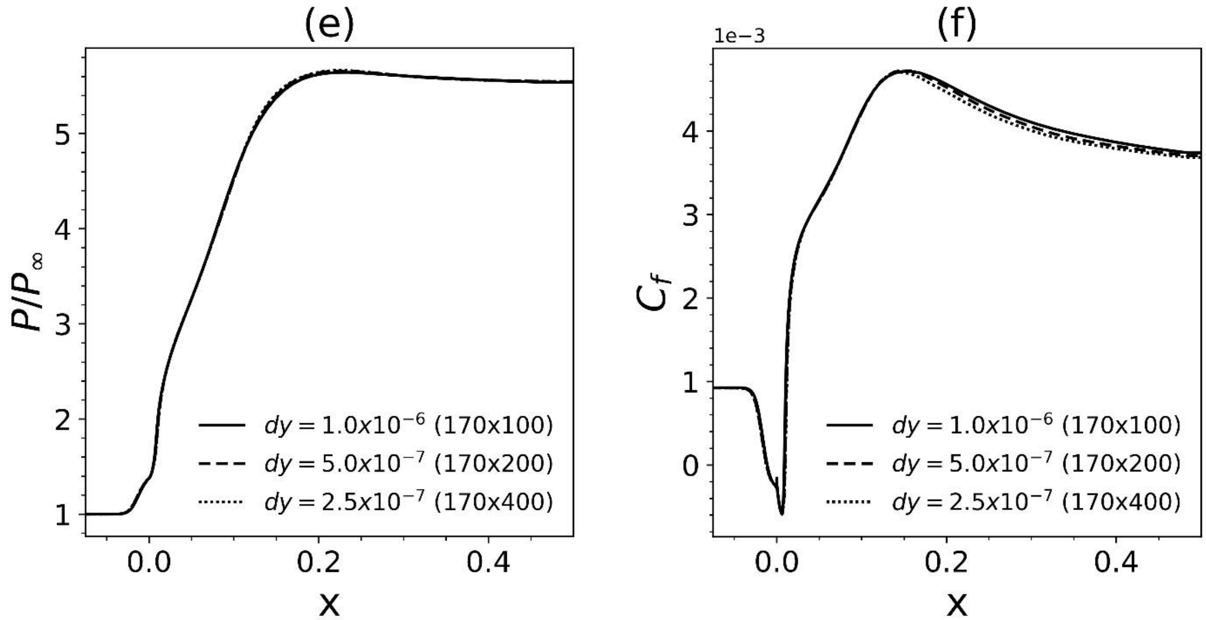

Figure 6 : Pressure and skin-friction plots showing grid convergence obtained by varying the (a,b) second ramp length (c,d) number of grid points in stream-wise direction and (e,f) number of grid points in wall-normal direction.

The optimum value of the first ramp length (R_1) and second ramp length (R_2) in the computational domain is obtained from the results plotted in figure-6a,b so that the separation bubble is well within the computational domain. Keeping the first ramp length constant, the second ramp is varied from 0.4 to 0.7 in steps of 0.10 m. Increasing the ramp length values above 0.5m does not much affect the results as seen from the pressure and skin-friction plots of figure-6a,b. For all the cases considered, the boundary layer thickness δ was with in the 0.04 m range. In figure-6c,d the number of grid points and the first grid thickness value is varied in stream-wise direction while that in figure-6e,f the number of grid points and the first grid thickness is varied in wall-normal direction. The domain is divided into 200 grid points in wall-normal direction and into 170 grid points in stream-wise direction.

The grid is clustered near the wall in wall-normal direction and near corner in stream-wise direction. As the number of points in stream-wise or wall-normal direction is halved/doubled, the value of first cell thickness in stream-wise or wall-normal direction is doubled/halved respectively for the grid-convergence study. Only for the coarse grid cases slight difference is observed at the peak values of skin-friction while for all other cases the difference is negligible. Based on the above study, the length of first ramp, second ramp and inlet in the computational domain is taken as 0.20 m, 0.50 m and 0.04 m respectively. The number of grid points in x-direction and y-direction is taken as 170 and 200 respectively while the first cell-thickness in y-direction and x-direction is taken to be 5 x 10^{-7} and 5 x 10^{-4} respectively for all simulations.

III. Results and discussions

A. EFFECT OF CANONICAL PARAMETERS

The results for the canonical parameters is presented followed by discussion and analysis of observed results

1. Effect of wall-temperature

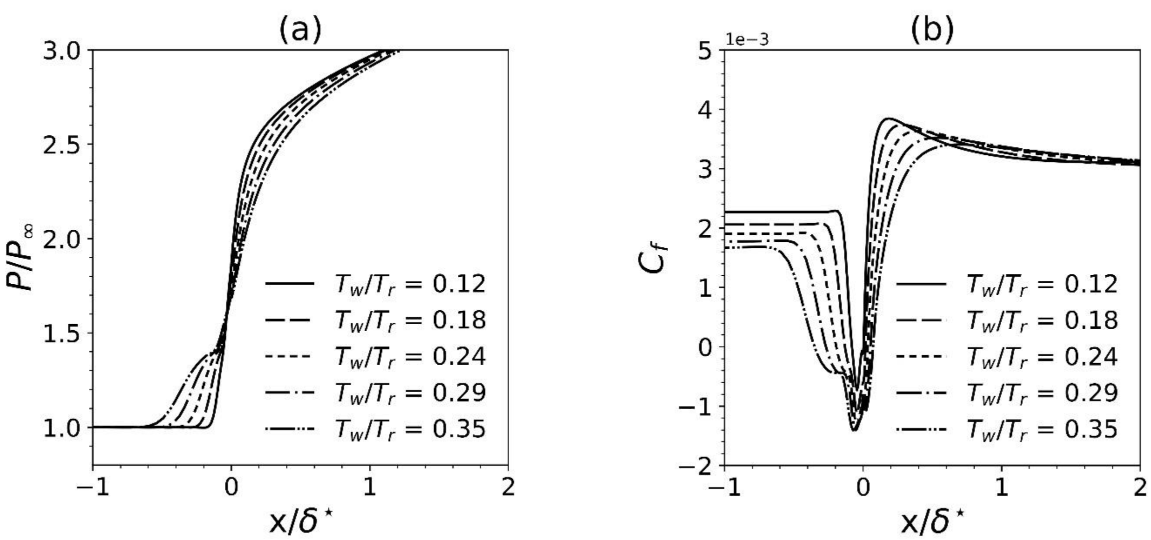

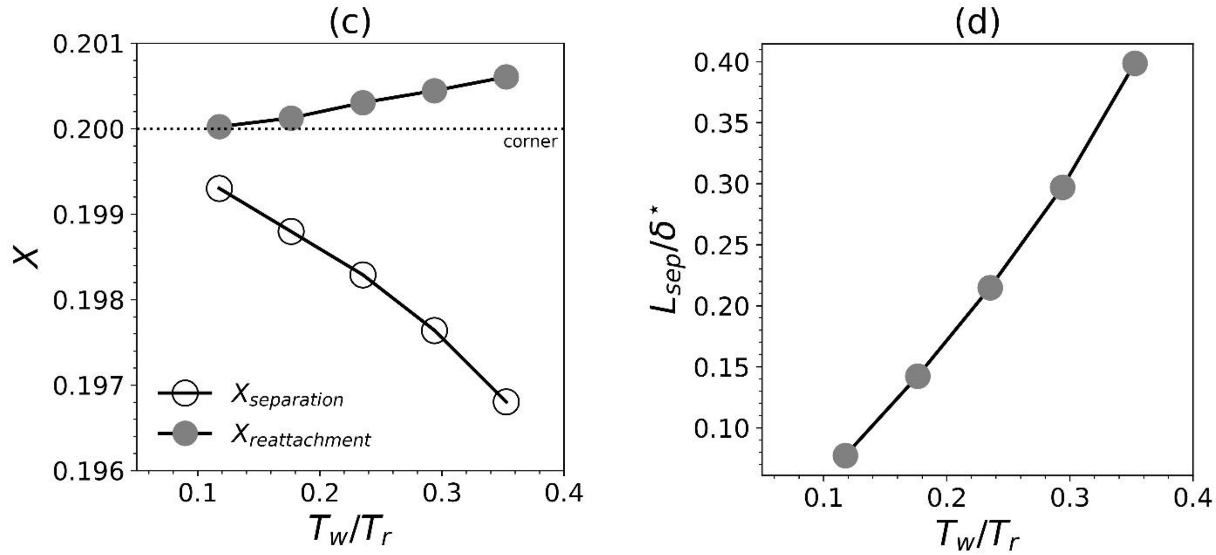

Figure 7 : (a) Distribution of wall-pressure, (b) distribution of skin-friction, (c) variation in separation and re-attachment points, and (d) variation in separation length normalized by δ* for different wall-to-recovery-temperature ratios.

The effect of wall-to-recovery-temperature ratio T_w/T_r on shock-boundary layer interaction over the compression ramp corner is studied. The free-stream conditions and flow deflection angle are kept constant with wall-temperature being varied as 200, 300, 400, 500 and 600 K which gives wall-to-recovery-temperature ratio as 0.12, 0.18, 0.24, 0.29 and 0.35 respectively for each case. Distribution of normalized mean pressure (normalized by pressure at upstream of start of interaction and is designated as P/P_∞ in all the figures) and mean skin-friction coefficient over the surface are presented in Figure-7a,b for a given range of wall-to-recovery-temperature ratios. For the lowest T_w/T_r ratio, the pressure rises just upstream of the corner which indicates start of flow-separation and this pressure rise is sharp and distributed over a very small region. As the T_w/T_r ratio increases, this pressure rise happens much upstream of the corner leading to increase in size of the separation bubble. The pressure rise is gradual and distributed over a region contrary to sharp rise seen for lower wall-temperatures. This shows the upstream influence increases with increase in wall-to-recovery-temperature ratio T_w/T_r.

Figure-7b presents the skin-friction distribution over the ramp surface for different wall-temperatures. The point where the x-location takes zero skin-friction value indicates the separation point (S) and start of flow-separation and the location where it comes back to zero value again from negative values indicate the re-attachment point (R). In the region between these two points (separation and re-attachment points), the flow is reversed and separation length is taken as the distance between these two points S and R. As the wall-temperature increases, both separation and re-attachment points move away from the corner (as shown in Figure-7c) and the separation length is found to increase as shown in Figure-7d. The reason for the observed trend is due to the changes in near-wall properties with wall-temperature changes and these in turn affect the boundary layer thickness and the subsonic channel thickness or sonic layer. Increase in wall-temperature leads to increase in near-wall viscosity which in turn leads to increase in boundary layer thickness δ. This leads to expansion of the subsonic channel thickness and since the separation bubble is always encompassed in the subsonic channel, it leads to increase in separation length. Further it can also be inferred that the increase in free-stream temperature should lead to a decrease in separation length as the ratio T_w/T_r decreases with increase in temperature. Similarly, pressure and density also have the same effect. John et al. [7] did a numerical study of various factor affecting shock-boundary layer interactions and commented that limited evidence available to show wall-to-total temperature would be a more relevant governing parameter for separation length studies. The results obtained in this work will be analyzed with respect to wall-to-recovery-temperature ratio to see if it can be the non-dimensional parameter for separation length analysis and its limitations

2. Effect of Mach number

The influence of Mach number on shock-boundary layer interaction phenomenon is studied. For on-design condition, the Mach number at station-2 is M_2= 4.097 whereas pressure, temperature and density are 6.5861 x 104 Pa, 426.55 K and 0.05385 kg/m^3respectively. Keeping all the parameters constant, the Mach number (or velocity as temperature is constant) is varied from M = 3 to 6 to study the effect of Mach number.

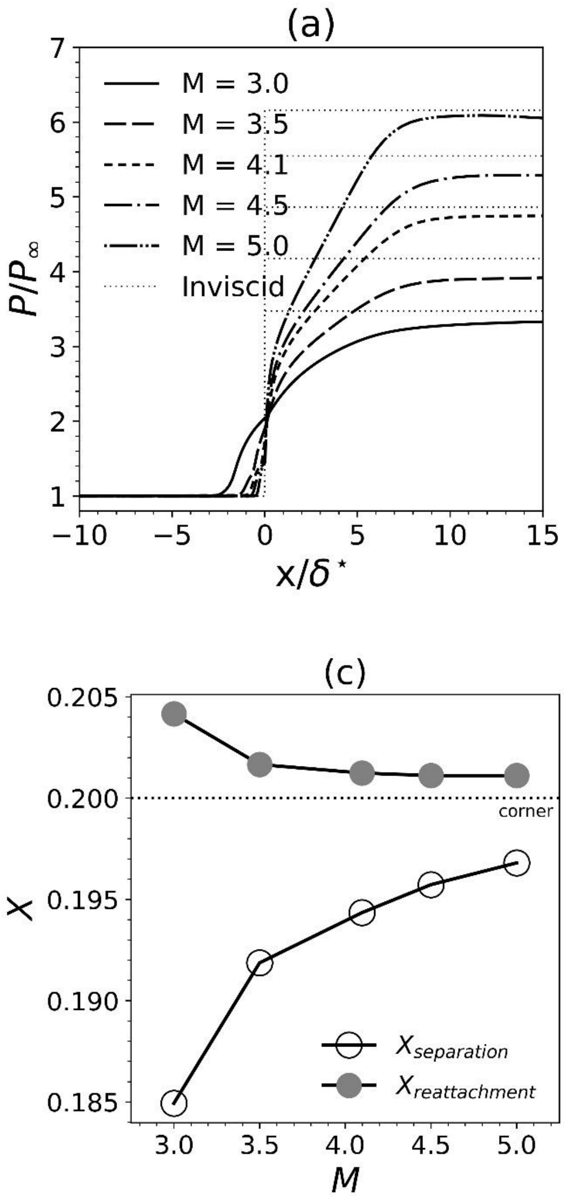

Figure 8 : (a) Distribution of wall-pressure, (b) distribution of skin-friction, (c) variation in separation and re-attachment points, and (d) variation in separation length normalized by δ* for different Mach numbers.

Figure-8a,b shows the distribution of mean wall pressure and mean skin-friction over the surface for a given range of Mach number variation. As the Mach number is increased, the pressure jump across the shock, as calculated using Rankine-Hugoniot relations, increases due to the increased shock-strength and is denoted by dotted lines in Figure-8a. The computed predictions show a close match and it is observed that upstream influence decreases with increase in Mach number *i.e.* the interaction length decreases with increasing Mach number leading to smaller separation. Further, as the Mach number increases both separation and re-attachment points are found to move closer towards the corner, as shown in Figure-8c, implying a decrease in separation length. Figure-8a gives comparison of the pressure rise for different Mach numbers with respective inviscid pressure jump indicated by dotted line. For higher Mach numbers, the pressure rises just upstream of the corner which indicates start of flow-separation. As the Mach number reduces, this pressure rise happens much upstream of the corner leading to increasing size of the separation bubble. As seen the pressure jumps are always lower than the respective inviscid values. For lower Mach numbers there is a very small difference in the computed and inviscid pressure rise. However, as the Mach number increases, this difference increases by a small amount. Further peak pressure is slightly higher than the inviscid values as Mach number increases which indicates the existence of turbulent flows. From Figure-8b which shows the skin-friction distribution for different Mach numbers, it is observed that the longest separation bubble is for the lowest Mach number and vice-versa. The value of skin-friction starts to decreases as it approaches the separation region, reaches to zero at separation point. It takes negative values in the separation bubble and comes reaches back to zero at reattachment point. After the re-attachment point, it increases beyond its free-stream values and then becomes constant after some distance. Thus, as the Mach number increases, the size of the separation bubble is found to decrease as shown in Figure-8d. Further, it is observed that this effect is analogous to wall-temperature study. As the Mach number increases, the separation length decrease and wall-to-recovery-temperature ratio is also found to decrease. This shows that increase in Mach number is analogous to wall-cooling as both wall-cooling and increase in in Mach number lead to decrease in separation length. Decrease in Mach number has an effect similar to wall-heating as both lead to increase in separation length.

3. Effect of Reynolds number

Numerical simulations are done for a range of Reynolds number Re_δ keeping the Mach number, flow-variables, wall-temperature and deflection angle constant. The range of Reynolds number (Re_δ = 6.0012 x 10^4, 7.2991 x 10^4, 8.8872 x 10^4, 1.0284 x 10^5, 1.1327 x 10^5) is obtained by varying the first ramp length such that for all the cases flow remains turbulent upstream of the interactions. Distribution of mean pressure and mean skin-friction over the surface is shown in Figure-9a,b for the given variation in Re_δ .

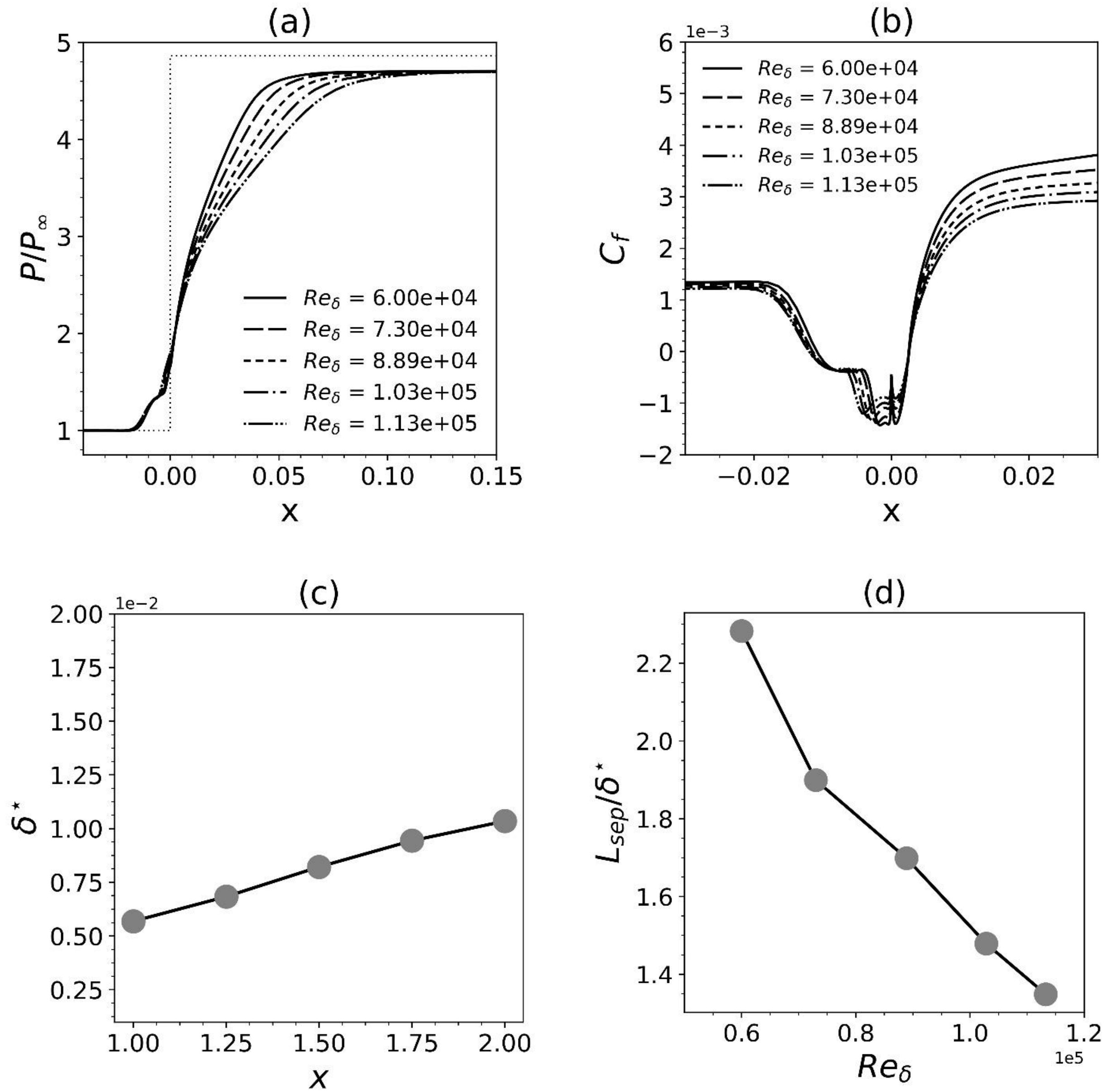

Figure 9 : (a) Distribution of wall-pressure, (b) distribution of skin-friction, (c) variation in displacement boundary layer thickness, and (d) variation in separation length normalized by δ* for different Reynolds number Re_{δ}.

From the simulation results, it is observed that the effect of Reynolds number Re_{δ} on the extent of interaction length is very small relatively as pointed by Holden et al [26]. Increase in Reynolds number Re_{δ} leads to a small rise in the upstream influence as seen in the magnified view of the region of interaction. From the skin-friction plot in Figure-9b it is observed that the separation points moves slightly away from the corner whereas the re-attachment point moves away from the corner by a very small amount leading to increase in separation length as observed by

Pasha et al. [5] . Even though the separation length increases by a small margin with the increase in Reynolds number Re_δ , the normalized separation length shows a reversal in trend. The reason being - changes in displacement boundary layer thickness (shown in figure-9c) is much larger compared to that in the separation length which leads to normalized separation length showing an opposite trend as seen in Figure-9d. The results in figure-9a,b are presented without normalizing the stream-wise direction to bring out the above observation. If the results in figure-9a,b were presented with stream-wise direction normalized, both upstream influence and separation length would reduce with increase in Reynolds number Re_δ .

B. EFFECT OF FLIGHT PARAMETERS

The result for the flight parameters is presented followed by discussion and the results are analyzed with respect to the wall-to-recovery-temperature ratio to see if it is the governing parameter for separation length studies. Further, the effect of shock-induced flow-separation on pressure forces acting on the intake ramp is discussed.

1. Effect of flight Mach number

Changes in flight Mach number makes the shock boundary layer interactions (SBLI) at the corner more complex as there are multiple parameters varying. As the flight Mach number at station-1 is varied from M_1= 4 to 8 (on-design condition is M_1= 6), the Mach number, pressure, temperature and density at station-2 changes as given in Table-1. The observed changes in separation length is result of cumulative effect of changes in these multiple parameters and this makes the analysis of results complicated as compare to canonical cases where only parameter is varied. Mean pressure and skin-friction distribution over the ramp surface for different flight Mach number is shown in Figure-10a,b.

Table 1 Conditions at station-2 for different flight Mach numbers.

M_1	M_2	p_2	ρ_2	T_2
4	2.99	4.08×10^{-4}	0.0416	341.74
5	3.58	5.23×10^{-4}	0.0478	380.91
6	4.10	6.57×10^{-4}	0.0538	426.55
7	4.53	8.18×10^{-4}	0.0595	478.93
8	4.90	9.99×10^{-4}	0.0647	538.31

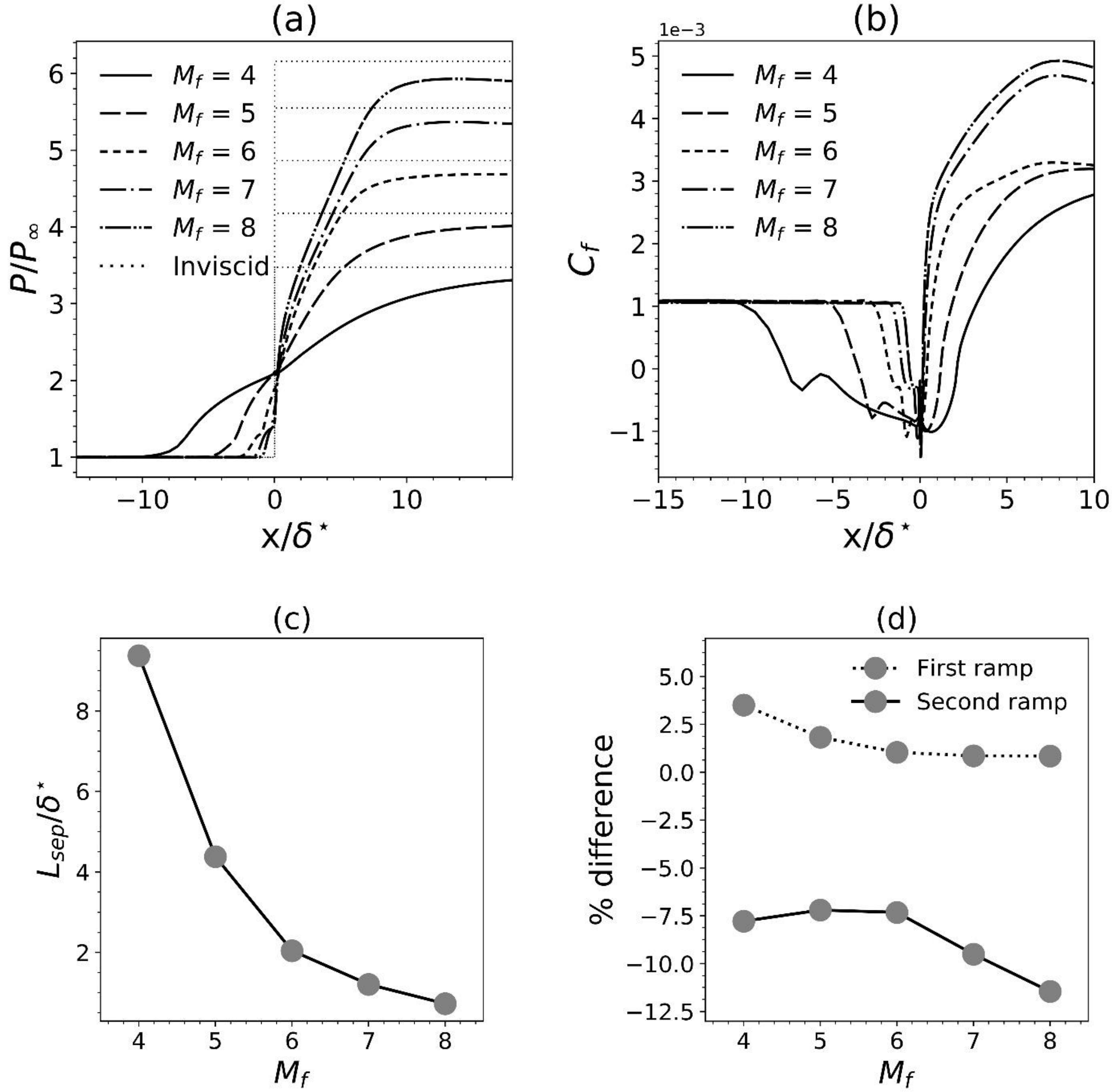

Figure 10 : (a) Distribution of wall-pressure, (b) distribution of skin-friction, (c) variation in separation length normalized by δ* and (d) % change in lift and drag forces acting over the two ramps for different flight Mach numbers.

The inviscid pressure rise across the shock for different flight Mach numbers is shown by dotted lines. The computed pressure distribution over the wall matches closely with the inviscid data. The upstream influence is found to be maximum for the lowest flight Mach number and minimum for the highest flight Mach number. Further, the computed pressure rise across the shock is always lower than the inviscid data for all cases. For lower flight Mach numbers there is a very small difference in the computed and inviscid pressure rise. However, as the flight Mach number increases, the difference between the computed and inviscid results keeps on increasing. From the skin-friction plot (Figure-10b) it is observed that increasing flight Mach number pushes the separation and re-attachment point closer towards the corner and thus reducing the separation length as seen in Figure-10c. This observed trend is similar to that obtained by varying Mach number in the canonical study and further, the results are analogous to effect of wall-to-recovery-temperature ratio *i.e.* high flight Mach number is similar to wall-cooling which leads to decrease in separation length and vice-versa. Table-2 shows the variation of T_w/T_r for different flight Mach numbers. As the flight Mach number increases, the ratio T_w/T_r decreases and separation length also decreases. Changes in separation length is inversely proportional to Mach number and the recovery temperature is a function of Mach number as $T_r = T\left(1 + \frac{\gamma-1}{2} rM^2\right)$. This shows wall-to-recovery-temperature ratio is a relevant parameter for separation length studies with respect to flight Mach number.

Table 2 Variation in wall-to-recovery-temperature ratio for different flight Mach numbers.

M_1	T_w	M_2	T_2	T_w/T_r
4	1700	2.98	341.74	1.92
5	1700	3.58	380.91	1.36
6	1700	4.09	426.55	1.00
7	1700	4.53	478.93	0.76
8	1700	4.90	538.31	60

Figure-10d shows the percentage difference between the inviscid and the computed values for Lift/Drag forces acting on the first ramp R_1 and second ramp R_2 for flight Mach numbers. Since the separation length decreases with the increase in flight Mach number, the percentage difference is also expected to decrease. For the first ramp, the percentage difference decreases with increase in flight Mach number whereas for the second ramp it decreases till M = 6 and then starts to increase (Negative change indicates the computed pressure is lower than the inviscid whereas positive change shows the computed pressure is higher than the inviscid). The reason for this is at higher Mach numbers (M = 7, 8), the computed pressure jump is much lower than the inviscid and the difference further increases with the increase in flight Mach number. Over the first ramp, the percentage difference is within 5% whereas over the second ramp it can be as high as 12% for highest of the off-design conditions. This high % difference for M = 8 case is due to two effects - (i) presence of separation bubble which modifies the pressure distribution across the corner for both ramps and (ii) pressure jump across the shock which is much lower than that obtained through Rankine-Hugoniot (inviscid) relations. The wall-pressure distribution over the first ramp is affected only by the separation bubble whereas that over the second ramp is affected by separation bubble as well as the pressure jump across the shock. Deviation in pressure jump across the shock is higher for higher Mach number with respect to analytical solution. This makes the deviation in pressure jump across the second ramp.

2. Effect of angle of attack

The effect of angle of attack on shock-boundary layer interaction is studied and its effect on separation length is analyzed in this section. As the angle of attack increases, the apparent first ramp angle θ_1^* changes given by $\theta_1^* = \theta_1 + \alpha$ where θ_1 is the first ramp angle and α is the angle of attack. Thus, as the angle of attack increases, the shock becomes stronger due to the increased apparent ramp angle. Due to the increased shock-strength, the Mach number at station-2 decreases whereas the flow-variables (p, T and ρ) at station-2 increases as given in Table-3. Numerical simulations are done to study the effect of angle of attack using conditions as given in Table-3. Mean wall-pressure and mean skin-friction distribution over the ramp surface is shown in Figure-11 for different angles of attack.

Table 3 Conditions at station-2 for different angles of attack.

α	M_2	p_2	ρ_2	T_2
-4	4.6237	4.3807×10^{4}	4.3349×10^{-2}	352.12
-2	4.3583	5.4123×10^{4}	4.8716×10^{-2}	387.11
0	4.0970	6.5881×10^{4}	5.3841×10^{-2}	426.35
2	3.8425	7.9086×10^{4}	5.8635×10^{-2}	469.96
4	3.5962	9.3724×10^{4}	6.3047×10^{-2}	517.97

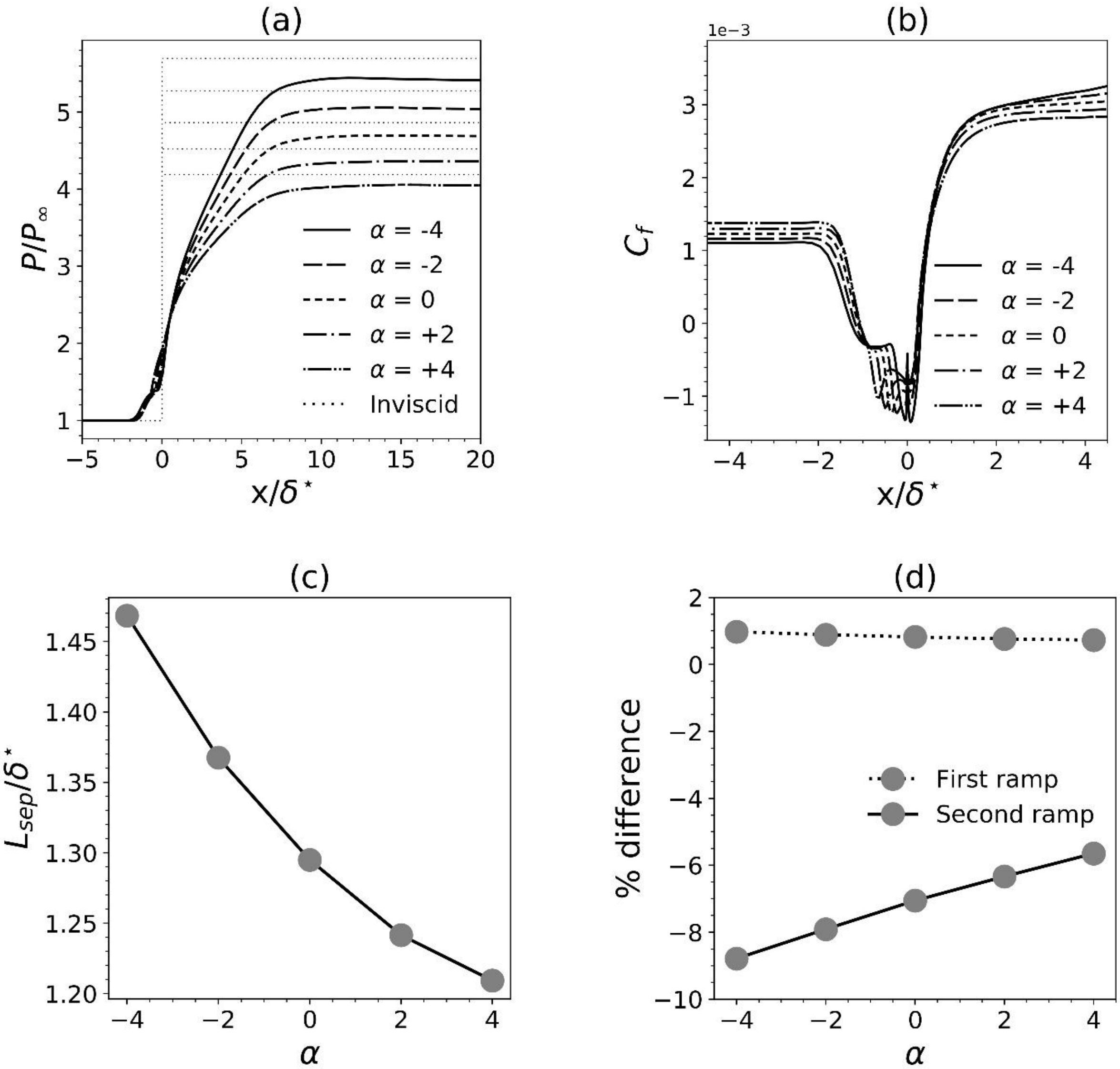

Figure 11 : (a) Distribution of wall-pressure, (b) distribution of skin-friction, (c) variation in separation length normalized by δ* and (d) % change in lift and drag forces acting over the two ramps for different angles of attack.

With increasing angle of attack, the shock-strength increases leading to increase in pressure jump across the shock and the computed wall-pressure distribution is compared with the inviscid solution as shown in Figure-11a. The upstream influence is found to decrease with an increase in angle of attack. From the skin-friction plot distribution, shown in Figure-11b, the separation and re-attachment point move closer towards the corner leading to a decrease in separation length as shown in Figure-11c. Wall-to-recovery temperature ratio is found to decrease with an increase in angle of attack as shown in Table-4. This shows an increase in angle of attack is analogous to wall-cooling leading to a decrease in separation length and vice-versa. Figure-11d shows a graphical representation of the percentage difference between the inviscid and the computed values for Lift/Drag forces acting on the first ramp R_1 and second ramp R_2 for different angles of attack. Since the separation length decreases with an increase in angle of attack, the percentage difference is also found to decrease.

Table 4 Variation in wall-to-recovery-temperature ratio for different angle of attack.

α	T_w	M_2	T_2	T_w/T_r
-4	1300	3.9562	517.97	0.76829
-2	1300	3.8425	469.96	0.76653
0	1300	4.0970	426.35	0.76462
+2	1300	4.3583	387.11	0.76243
+4	1300	4.6237	352.12	0.76008

3. Effect of cruise altitude

The influence of variation in cruise altitude on separation length is explored in this section. For the range of altitude (26 km to 34 km) considered in the current study, the pressure and density decreases whereas the temperature increases. Since the Mach number is constant, the shock-strength remains same for all cases and only changes occurring are in pressure, temperature and density at station-2 as given in Table-5. Numerical simulations were done to study the effect of altitude on flow-separation keeping all parameters constant and varying the flow-properties as given in Table-5.

Table 5 Conditions at station-2 for different altitude.

z	M_2	p_2	ρ_2	T_2
26	4.097	1.2311×10^4	0.10242	418.74
28	4.097	9.0923×10^4	0.07498	422.51
30	4.097	6.5922×10^4	0.05385	426.55
32	4.097	5.0019×10^4	0.04051	430.03
34	4.097	3.7326×10^4	0.02956	439.82

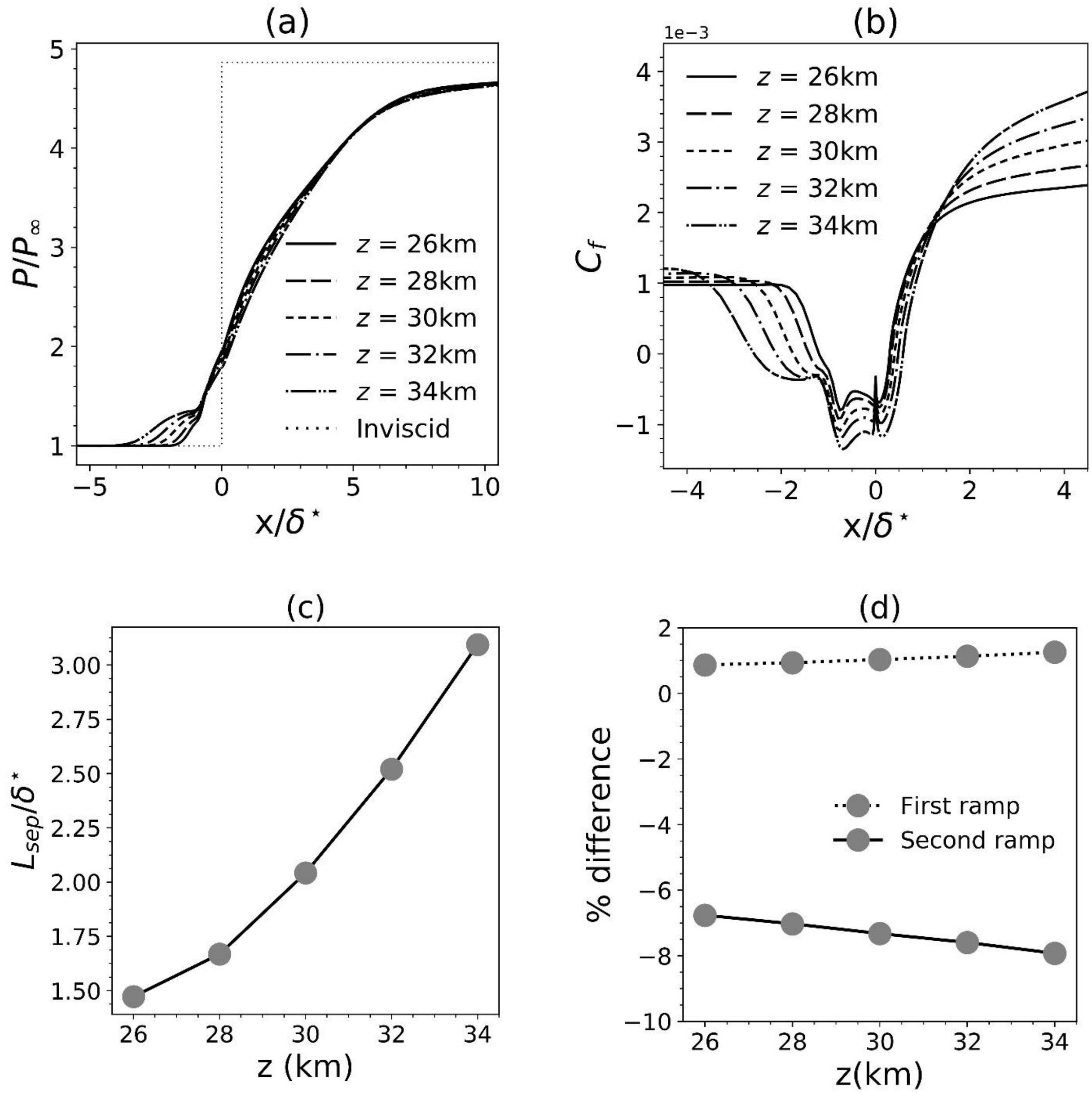

Figure 12 : (a) Distribution of wall-pressure, (b) distribution of skin-friction, (c) variation in separation length normalized by δ* and (d) % change in lift and drag forces acting over the two ramps for different altitudes.

Figure-12a shows the wall-pressure distribution for different altitudes. Since the Mach number is kept constant for all cases, the shock-strength remains same and hence the pressure jump is same for all altitudes. The upstream influence is found to increase with increase in altitude leading to increase in separation length. From the skin-friction plot shown in Figure-12b, the separation and re-attachment point are found to move away from the corner with increase in altitude implying increase in separation length as shown in Figure-12c. On analyzing the observed results with respect of wall-to-recovery-temperature ratio, it is found that as the altitude increases the ratio T_w/T_r decreases whereas the separation length is found to increase. Thus, the wall-to-recovery-temperature ratio, which was found to scale linearly with separation length for all parameters studied till now, fails to be the governing parameter for the separation length study with respect to changes in altitude. The probable reason for this is, although the recovery temperature T_r takes into account the changes in upstream temperature and Mach number, the ratio T_w/T_r fails to take into account the changes in upstream density and or pressure. As the altitude increases, all three parameters -pressure, temperature and density - are changing and further the variation in pressure and density is opposite to that of temperature. Hence the ratio T_w/T_r fails to scale with separation length changes. Figure-12d shows the graphical representation of percentage difference between the inviscid and the computed values for Lift/Drag forces acting on the first ramp R_1 and second ramp R_2 for different altitudes. It is seen that the maximum percentage difference over the first ramp is around 2% whereas that over the second ramp is around 8% for all the given cases.

Table 6 Variation in wall-to-recovery-temperature ratio for different cruise altitude.

M_1	T_w	M_2	T_2	T_w/T_r
26	1700	3.9562	418.74	1.0180
28	1700	3.8425	422.51	1.0090
30	1700	4.0970	426.55	0.9994
32	1700	4.3583	430.03	0.9913
34	1700	4.6237	439.82	0.9693

IV. Conclusion

In this paper, we study shock-induced flow-separation and how it varies with respect to canonical and flight parameters. From the study of canonical parameters it is observed that the separation length increases with increase in wall-to-recovery-temperature ratio and Reynolds number Re_δ whereas with respect to Mach number it shows an opposite effect. The changes in separation length with respect to Reynolds number is very small and the normalized separation length shows a trend reversal since the changes in displacement boundary layer thickness are much higher compared to changes in separation length. From the study of flight parameters it is observed that the separation length increases with increase in cruise altitude whereas it decreases with increase in angle of attack and flight Mach number. Changes in Mach number is found to be analogous to changes in wall-to-recovery-temperature ratio. Increase in Mach number has similar effect on separation as wall-cooling and vice-versa. We next analyze the effect of flight conditions on separation length. As the flight Mach number and angle of attack increases, separation length decreases and wall-to-recovery-temperature ratio is also found to follow the same trend. However, changes in separation length due to altitude variation does not scale with wall-to-recovery-temperature ratio and the probable reason for this might be that the wall-to-recovery-temperature ratio does not take into account the changes in upstream density and or pressure. The inviscid pressure lift and drag forces are compared with the computed lift and drag forces to find the percentage difference between the two and identify the worst case scenario. The off-design condition operation of M = 8 is found to be the worst case scenario where the percentage difference can be as high as 12%.

V. References

1. Marini, Marco. "Effects of flow and geometry parameters on shock-wave boundary-layer interaction phenomena." *8th AIAA International Space Planes and Hypersonic Systems and Technologies Conference*. 1998.
2. Verma, S. B., and A. Hadjadj. "Supersonic flow control." *Shock Waves* 25 (2015): 443-449.
3. Babinsky, Holger, and John K. Harvey, eds. *Shock wave-boundary-layer interactions*. Vol. 32. Cambridge University Press, 2011.
4. Gaitonde, Datta V. "Progress in shock wave/boundary layer interactions." *43rd AIAA Fluid Dynamics Conference*. 2013.
5. Pasha, Amjad Ali. "Study of Parameters Affecting Separation Bubble Size in High Speed Flows using k-ω Turbulence Model." *Journal of Applied and Computational Mechanics* 4.2 (2018): 95-104.
6. Bernardini, Matteo, et al. "Heat transfer and wall temperature effects in shock wave turbulent boundary layer interactions." *Physical Review Fluids* 1.8 (2016): 084403.
7. John, Bibin, Vinayak N. Kulkarni, and Ganesh Natarajan. "Shock wave boundary layer interactions in hypersonic flows." *International Journal of Heat and Mass Transfer* 70 (2014): 81-90.
8. Morgan, Brandon, Soshi Kawai, and Sanjiva Lele. "A parametric investigation of oblique shockwave/turbulent boundary layer interaction using LES." *41st AIAA Fluid Dynamics Conference and Exhibit*. 2011.

9. Marini, Marco. "Analysis of hypersonic compression ramp laminar flows under sharp leading edge conditions." *Aerospace science and technology* 5.4 (2001): 257-271.

10. Katzer, Edgar. "On the lengthscales of laminar shock/boundary-layer interaction." *Journal of Fluid Mechanics*206 (1989): 477-496.

11. Roshko, A., and G. J. Thomke. "Flare-induced interaction lengths in supersonic, turbulent boundary layers." *AIAA Journal* 14.7 (1976): 873-879.

12. Elfstrom, G. M. "Turbulent hypersonic flow at a wedge-compression corner." *Journal of fluid Mechanics* 53.1 (1972): 113-127.

13. Needham, D., and John Stollery. "Boundary layer separation in hypersonic flow." *3rd and 4th Aerospace Sciences Meeting*. 1966.

14. Childs, M. E., R. Hijman, and D. S. Miller. "Mach 8 to 22 studies of flow separations due to deflected control surfaces." *AIAA Journal* 2.2 (1964): 312-321.

15. Sinha, Krishnendu, Krishnan Mahesh, and Graham V. Candler. "Modeling the effect of shock unsteadiness in shock/turbulent boundary-layer interactions." *AIAA journal*43.3 (2005): 586-594.

16. Oliver, Anthony, et al. "Assessment of turbulent shock-boundary layer interaction computations using the OVERFLOW code." *45th AIAA Aerospace Sciences Meeting and Exhibit*. 2007.

17. Sinha, Krishnendu, Krishnan Mahesh, and Graham V. Candler. "Modeling shock unsteadiness in shock/turbulence interaction." *Physics of Fluids* 15.8 (2003): 2290-2297.

18. Wilcox, David C. *Turbulence modeling for CFD*. Vol. 2. La Canada, CA: DCW industries, 1998.

19. Sinha, Krishnendu, and Vighnesh Pawar. "Shock/turbulence interaction: turbulence modeling and scramjet application." *11th Annual AeSI CFD Symposium, Indian Institute of Science, Bangalore, India*. 2009.

20. Sinha, Krishnendu, Nilesh J. Rane, and Vighnesh Pawar. "Numerical Investigation of three Dimensional shock/boundary-layer interaction in a hypersonic inlet." *28th International Symposium on Shock Waves, The University of Manchester, United Kingdom*. 2011.

21. Steger, Joseph L., and R. F. Warming. "Flux vector splitting of the inviscid gasdynamic equations with application to finite-difference methods." *Journal of computational physics* 40.2 (1981): 263-293.

22. Wright, Michael James. "A family of data-parallel relaxation methods for the Navier-Stokes equations." (1997).

23. Menter, Florian R. "Two-equation eddy-viscosity turbulence models for engineering applications." *AIAA journal* 32.8 (1994): 1598-1605.

24. Settles, Gary S., Thomas J. Fitzpatrick, and Seymour M. Bogdonoff. "Detailed study of attached and separated compression corner flowfields in high Reynolds number supersonic flow." *AIAA journal* 17.6 (1979): 579-585.

25. Souverein, L. J., P. G. Bakker, and P. Dupont. "A scaling analysis for turbulent shock-wave/boundary-layer interactions." *Journal of Fluid Mechanics* 714 (2013): 505-535.

26. Holden, Michael. "Measurements in Regions of Shock Wave/Turbulent Boundary Layer Interaction From MACH 4 to 7 at Flight Duplicated Velocities to Evaluate and Improve the Models of Turbulence in CFD Codes." *2018 Fluid Dynamics Conference*. 2018.